Molecular Orientation in Liquid Crystal Elastomers

Eric Anglaret,[†] Monique Brunet,[†] Bernard Desbat,[‡] Patrick Keller,[§] and Thierry Buffeteau*[,‡]

Laboratoire de Physico-Chimie Moléculaire (UMR 5803-CNRS), Université Bordeaux 1, 351 Cours de la Libération, 33405 Talence, France, Groupe de Dynamique des Phases Condensées (UMR 5581-CNRS), Université Montpellier 2, place E. Bataillon, 34095 Montpellier, France, and Laboratoire Physico-Chimie Curie (UMR 168-CNRS), Institut Curie−Section de Recherche, 11 rue P. et M. Curie, 75231 Paris, France

Received January 21, 2005; Revised Manuscript Received March 29, 2005

ABSTRACT: Free-standing and confined anisotropic liquid crystal elastomer films of various thicknesses have been prepared using mesogens with laterally affixed polymerizable side chains. Textures have been studied by microscopy, whereas molecular orienation of the mesogen groups has been investigated by polarized FTIR and Raman spectroscopies considering an uniaxial orientation of their long molecular axis with respect to the rubbing direction. Attenuated total reflectance (ATR) experiments have clearly shown a higher orientation of the mesogen groups near the film surface due to the anchoring effect of the rubbing layer. Inside the polymer, we have shown from transmittance experiments that the mesogens move away from the rubbing direction with a non cylindrical symmetry. In addition, a distribution function with a maximum at 48° from the rubbing direction has been calculated from the $\langle P_2 \rangle$ and $\langle P_4 \rangle$ order parameters obtained by polarized Raman spectra. The FTIR study of partially deuterated polymer films has shown that the backbone orientation along the rubbing direction is good inside the polymer whereas it is poor near the surface where the mesogens are well oriented. All these results suggest that the backbone orientation is constrained by the mesogen one. The nonhomogeneous mesogen orientation near the surface of the film is also featured by disclination lines observed by microscopic observations. Finally, experiments performed at different temperatures evidence a cylindrical symmetry of the mesogens above the nematic−isotropic transition temperature, a residual mesogen orientation in the isotropic phase and a mesogen orientation memory in the nematic phase.

Introduction

Liquid crystalline elastomers (LCEs), introduced as a theoretical concept by de Gennes in 1969,[1] have now become a reality.[2,3] These materials, which are "solid liquid crystals", are currently the subject of intense studies due to their scientific interest and also potential technological applications. In particular, the possibility of using a LCE as an artificial muscle was first suggested by de Gennes.[4] Since then, ordered LCEs have been shown to change reversibly dimensions under low stress through phase transitions and retain network memory.[5−7]

These systems make use of a conformational change of the polymer backbone at the nematic to isotropic phase transition as the motor for a macroscopic contraction. For side-on liquid crystalline polymers, this anisotropy of conformation of the polymer backbone in the nematic phase results from a strong coupling between the mesomorphic order imposed by the mesogenic side groups and the polymer chain.[8] The change of the sample size observed when the system passes through the nematic−isotropic transition is obviously correlated with a large reorientation of some molecular groups. However, the orientational mechanism occurring during the contraction is not straightforward.

Microscopy is often used to get information on the molecular arrangement in liquid crystals. Indeed, topological defects can be observed by microscopy indicating the presence of domains or discontinuities which can be sometimes associated with molecular reorientations. To interpret the microscopic observations, liquid crystal molecules are treated as rigid rods in most theoretical models. This molecular view for liquid crystalline elastomer is certainly incorrect since both the backbone, the spacer and the mesogen can play an important role in the reorientation mechanism.

Spectroscopic techniques can be used as complementary and powerful research tools in studying selectively the different molecular groups of the polymer. Polarized FTIR spectroscopy has been used to determine the molecular orientation of different functional groups of LCE samples.[9] In transmittance experiments at normal incidence, the orientational information concerns the sample on the whole since the infrared radiation probes all the thickness of the polymer film. Therefore, only thin films can be investigated to prevent saturation of the more intense absorption bands. To overcome this limitation, polarized attenuated total reflectance (ATR) can be used since only a small part of the thickness of the sample interacts with the evanescent wave occurring in ATR experiments.[10] More interestingly, ATR can be used as a surface characterization. By using a high refractive index of the crystal (germanium for example), it is possible to study the molecular orientation near the surface of the polymer films (the thickness probed is smaller than 0.5 μm).

To quantify the molecular orientation, it is necessary to define an orientational model. For liquid crystal

* Corresponding author.
[†] Université Montpellier 2.
[‡] Université Bordeaux 1.
[§] Institut Curie−Section de Recherche.

10.1021/ma050136n CCC: $30.25
Published on Web 04/27/2005

Scheme 1. Chemical Formula of the 4″-Acryloyloxybutyl 2,5-Di(4′-butyloxybenzoyloxy) Benzoate Monomer

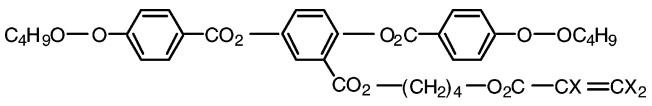

1a X= H

1b X= ^{2}H

molecules, an uniaxial orientation of the mesogen with respect to the rubbing direction is generally considered. The molecular orientation can be defined by an orientation function distribution that can be expanded in a series of even Legendre polynomials. FTIR spectroscopy gives only the second term $\langle P_2 \rangle$ of the Legendre polynomial series. On the other hand, polarized Raman scattering can provide more precise information about the molecular orientation since the first two order parameters $\langle P_2 \rangle$ and $\langle P_4 \rangle$ can be calculated. Thus, this technique has been often used to investigate the molecular orientation in liquid crystals.[11−14]

In this paper, the backbone and the mesogen orientations of LCE films have been investigated by FTIR and Raman spectroscopies in the nematic state and at the nematic−isotropic transition. An orientational model is proposed to interpred both microscopic and spectroscopic results.

Experimental Section

Anisotropic LCE film Preparation. Monomers **1a** and **1b**, whose chemical structures are shown in Scheme 1, were prepared according to methods detailed previously.[6,15] First 90 mol % of **1a** (or **1b**) and 10 mol % of 1,6-hexanediol diacrylate mixture was used for the preparation of aligned LCE samples. Mixtures were filled in rubbed poly(vinyl alcohol) (PVA) coated glass cells of various gaps at 100 °C. The filled cells were cooled under nitrogen at −1 °C/min down to 70 °C (nematic mesophase) to achieve alignment.

Photopolymerization of the mixture has been induced by UV light (Teklite ELC 400, 10 mn light exposure at 365 nm using an irradiance of 25 mW/cm^2) in the nematic state. Below 5 μm the glass substrates are glued without spacers, and are only assembled together by clips. Beyond 5 μm, Mylar spacers define the film thickness. The thickness of the cell is calculated, before filling, from the interference fringes measured with a UV−visible spectrometer. The error is about 0.5 μm for thin gaps (<10 μm) and 1−2 μm for thick gaps (>10 μm).

Free-standing films (typical size 2 cm × 1 cm) were obtained by dipping the glass cells for a few hours in a 40% HF solution, thus removing completely the glass windows without attacking the polymer. For in situ FTIR experiments, i.e., on films contained in cells, glass windows were replaced by ZnS or BaF_2 window cells.

Microscopy. Microscopic observations have been performed using a polarizing microscope with crossed polarizers (Leica, Laborlux 12 POL S). To measure distances in the field of the microscope, we used a micrometric eyepiece calibrated for each objective which provides a high accuracy. To work in the best conditions of flatness, the films have been observed either confined between the substrates, or after removing the top plate, specially at high magnification.

Spectroscopic Measurements. Transmittance and ATR infrared spectra were recorded on a Magna 560 (Nicolet) FTIR spectrometer equipped with a germanium coated KBr beam splitter and a HgCdTe (MCT) detector cooled at 77 K. A ZnSe wire-grid polarizer (Specac) was positioned in front of the sample to obtain polarized spectra. For ATR spectra, the "Silver gate" accessory (Eurolabo) with germanium crystal (refractive index of 4.0) and only one reflection at an incidence angle of 45° was used. To obtain polarized ATR spectra, the infrared beam was polarized perpendicular to the incidence plane and the sample was positioned with the rubbing direction parallel or perpendicular to the polarization direction. A total of 1000 scans was sufficient to achieve a high signal-to-noise ratio. The spectrometer and the ATR accessory were purged with dry air to minimize water vapor. For polarized transmittance spectra, the infrared beam passed through the sample at normal incidence and was polarized parallel or perpendicular to the rubbing direction. For each measurement a total of 1000 scans were averaged at a resolution of 4 cm^{-1}. The polarized transmittance spectra were recorded at room temperature on free-standing films in the nematic state. Additional experiments were performed at different temperatures on films placed between BaF_2 plates having rubbed PVA surface. The polarized spectra were collected in both the nematic and isotropic phases after stabilizing the temperature for 10 min before each new measurement, using an homemade heating cell associated with a WEST 6100 hot stage temperature controller.

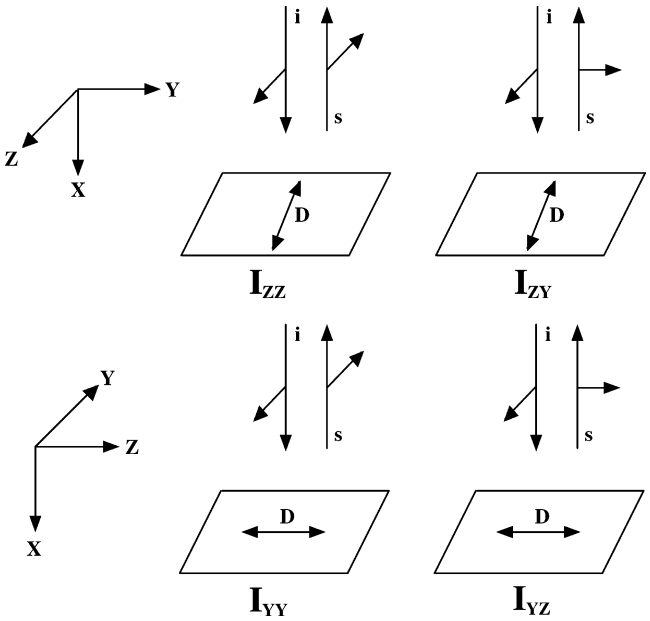

Figure 1. Sketch of the four different experimental configurations I_{ZZ}, I_{ZY}, I_{YZ}, and I_{YY} used for the measurement of the Raman depolarization ratios. The first subscript refers to the polarization of the incident light and the second to that of the scattered light. The rubbing direction D is along the Z axis. The longer arrows indicate the direction of the incident (i) and scattered (s) light, and the shorter arrows show the polarization.

The Raman experiments were carried out on a Jobin-Yvon T64000 spectrometer using the 514.5 nm line of an Ar laser. All measurements were performed in a backscattering configuration using a microscope with an objective 50X (numerical aperture = 0.5). This objective allows an theoretical radial separation (minimum diameter of the light spot) of 1.26 μm and an theoretical depth of focus (axial resolution) of about 8 μm.[16] For the measurement of the depolarization ratio, the polarization of the incident beam was vertical (V) and an analyzer placed behind the sample was used to select the vertical (VV configuration) or horizontal (VH configuration) component of the scattered beam. The alignment direction can be parallel to the laser polarization (ZZ and ZY measurements) or perpendicular (YY and YZ polarizations), as sketched in Figure 1. When depolarization ratio are measured with a dispersive spectrometer, using anisotropic gratings, one must carefully consider the difference in the efficiency of the measurements of VV and VH intensities. To get free of the anisotropy of the gratings, a $\lambda/2$ wave-plate was placed behind the analyzer so that the polarization of the scattered beam made an angle of 45° with respect to the vertical axis for both

Scheme 2. Space Coordinate System (*X*, *Y*, *Z*), Molecular Coordinate System (*u*, *v*, *w*), Transition Moment (*M*), and the Euler Angles Used to Describe Biaxial Orientation

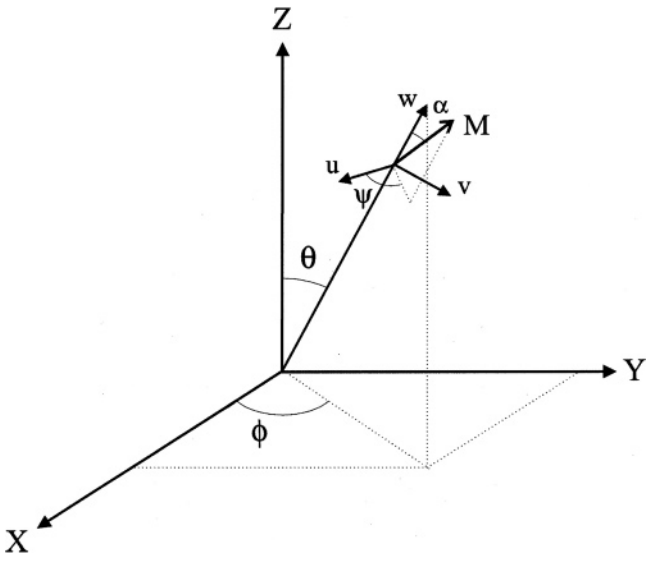

VV and VH configurations. In addition, we used an unpolarized white beam to determine the (frequency-dependent) correction factor for the setup sensibility for vertical and horizontal orientations of the analyzer. Using such a setup and correction factor, we checked that the polarization measurements for an isotropic liquid crystal were consistent, i.e., that the order parameters were zero. Finally, some series of measurement were performed using a confocal setup in order to probe the depth dependence of the depolarization ratio, i.e., of the orientational order.

Theoretical Part

The orientation of a transition moment **M** can be described with respect to the space coordinate system by using the Euler angles as shown in Scheme 2. The space coordinate system is formed by the *X*, *Y*, and *Z* axes where *Z* defines the rubbing direction *D* and *X* is normal to the film plane. The *u*, *v*, and *w* axes form the molecular coordinate system in which *w* is the long molecular axis of the mesogens and (*v*,*w*) defines the plane of the aromatic rings. The orientation of the long molecular axis, *w*, with respect to the space coordinate system is described by two Euler angles, the tilt (θ) and azimuthal (ϕ) angles, and the orientation of a transition moment with respect to the long molecular axis is defined by the α angle and by the third Euler angle, the twist angle (ψ). Using the system of axes defined in Scheme 2 and the transformation matrix given by Zbinden,[17] the components of the transition moment are given by

$$M_X = (\cos\psi\cos\theta\cos\phi + \sin\psi\sin\phi)M\sin\alpha + \sin\theta\cos\phi\, M\cos\alpha \quad (1a)$$

$$M_Y = (\cos\psi\cos\theta\sin\phi - \sin\psi\cos\phi)M\sin\alpha + \sin\theta\sin\phi\, M\cos\alpha \quad (1b)$$

$$M_Z = -\cos\psi\sin\theta\, M\sin\alpha + \cos\theta\, \mathrm{M}\cos\alpha \quad (1c)$$

where *M* is the absolute magnitude of the transition moment.

Considering that the extinction coefficients along each coordinate axis are proportional to the square of the transition moment and assuming an uniaxial orientation of the long molecular axis of the mesogens with respect to the rubbing direction (integration over the ϕ angle), we easily obtain the expression of the extinction coefficients in the space coordinate system:

$$k_X = k_Y = \frac{k_{\max}}{2}[\cos^2\psi\cos^2\theta\sin^2\alpha + \sin^2\psi\sin^2\alpha + \sin^2\theta\cos^2\alpha] \quad (2a)$$

$$k_Z = k_{\max}[\cos^2\psi\sin^2\theta\sin^2\alpha + \cos^2\theta\cos^2\alpha] \quad (2b)$$

where $k_{\max}$ is the maximum extinction coefficient, which is given for each wavenumber by the sum of k_X, k_Y, and k_Z.

The orientation of the liquid crystal mesogens with respect to the rubbing direction can be determined from the different infrared bands, using the dichroic ratio calculated from the polarized transmittance spectra, which is defined by

$$R^{\mathrm{T}} = \frac{A_{\parallel}}{A_{\perp}} = \frac{\langle k_Z\rangle}{\langle k_Y\rangle} \quad (3)$$

where $A_{\parallel}$ and $A_{\perp}$ are the absorbance for a radiation polarized parallel and perpendicular to the rubbing direction, respectively. For a transition moment parallel to the long molecular axis of the mesogens ($\alpha = 0°$), corresponding for example to the C=C stretching vibrations of the phenyl rings, the dichroic ratio is given by

$$R^{\mathrm{T}}_{(\alpha=0)} = \frac{2\langle\cos^2\theta\rangle}{\langle\sin^2\theta\rangle} \quad (4)$$

where $\langle\cos^2\theta\rangle$ and $\langle\sin^2\theta\rangle$ are the mean values of $\cos^2\theta$ and $\sin^2\theta$ for a distribution of transition moment in the film. It is noteworthy that the twist angle ψ does not appear in eq 4. The dichroic ratio of such bands therefore gives the tilt angle θ directly. Assuming a infinitely narrow distribution of the transition moment orientation, eq 4 can be rearranged to calculate θ:

$$\theta = \arctan\sqrt{\frac{2}{R^{\mathrm{T}}_{(\alpha=0)}}} \quad (5)$$

For a transition moment perpendicular to the long molecular axis of the mesogens ($\alpha = 90°$), corresponding for example to out-of-plane C−H deformation vibrations of the phenyl rings, the corresponding dichroic ratio calculated from the polarized transmittance spectra is given by:

$$R^{\mathrm{T}}_{(\alpha=90)} = \frac{2\langle\cos^2\psi\sin^2\theta\rangle}{\langle\cos^2\psi\cos^2\theta\rangle + \langle\sin^2\psi\rangle} \quad (6)$$

If the tilt angle is previously determined using a band with a transition moment along the long molecular axis and assuming an infinitely narrow distribution of orientation, the twist angle ψ can be calculated by the relation:

$$\psi = \arccos\sqrt{\frac{R^{\mathrm{T}}_{(\alpha=90)}}{[R^{\mathrm{T}}_{(\alpha=90)} + 2]\sin^2\theta}} \quad (7)$$

The twist angle ψ defines the orientation of the phenyl ring plane with respect to the film plane. $\psi < 45°$ corresponds to phenyl ring plane rather parallel to the film plane whereas $\psi > 45°$ corresponds to phenyl ring plane rather perpendicular to the film plane. The particular case of $\psi = 45°$ corresponds to a cylindrical symmetry of the mesogens with respect to the long molecular axis.

For ATR experiments, since the same polarization (perpendicular to the incidence plane) was used to record the two polarized spectra (only the sample was rotated between the two experiments), the dichroic ratio R^{ATR} can be calculated from the polarized ATR spectra by the relation

$$R^{ATR} = \frac{\log(1/R_{\perp}^{D|E})}{\log(1/R_{\perp}^{D\perp E})} = \frac{\langle k_Z \rangle}{\langle k_Y \rangle} \tag{8}$$

where $\log(1/R_{\perp}^{D|E})$ and $\log(1/R_{\perp}^{D\perp E})$ are the ATR spectra in absorbance for a radiation polarized perpendicular to plane of incidence and for the sample positioned with the rubbing direction D parallel and perpendicular to the polarization direction E, respectively. The dichroic ratios R^{ATR} and R^{T} are related to the anisotropic extinction coefficients $\langle k_Y \rangle$ and $\langle k_Z \rangle$ by the same equation, so that the relations 4−7 can be also used for ATR experiments. However, there is a difference between the results obtained via ATR and those obtained via conventional transmittance due to the particular character of the evanescent wave occurring in ATR experiments. Indeed, in conventional transmittance the whole thickness of the sample is probed by the infrared radiation, whereas in ATR only a thin layer of the sample interacts with the evanescent wave since the electric field amplitude of the evanescent wave decays exponentially with distance from the surface. To assess the penetration of the exponential field normal to the surface, Harrick et al.[18] defined the depth of penetration d_p as the distance required for the electric field amplitude to fall to 1/e of its value at the surface. This parameter d_p is given by the relation:

$$d_p = \frac{\lambda}{2\pi n_1 \sqrt{(\sin^2 \Phi - {n_{21}}^2)}} \tag{9}$$

where Φ is the angle of incidence, λ is the wavelength, n_1 is the refractive index of the ATR crystal, n_2 is the refractive index of the film, and $n_{21} = n_2/n_1$. It is noteworthy that the maximum depth sampled is about three times d_p; however, at this distance the electric field amplitude is only 5% of its value at the surface, and a major fraction of the information is obtained from shallower depths in the surface. Moreover, the absorption of the rarer medium is not taken into account in eq 9. Thus, the depth of penetration d_p is certainly more indicative of the probed thickness of the sample than $3d_p$.

Assuming an uniaxial orientation of the mesogens with respect to the rubbing direction, the orientation distribution of the long molecular axis, $f(\theta)$, can be characterized by using a series of Legendre polynomials, $P_l(\cos\theta)$:[19,20]

$$f(\theta) = \sum_{l=0}^{\infty} \left(\frac{2l+1}{2}\right) \langle P_l \rangle P_l(\cos\theta) \tag{10}$$

where the normalization term $(2l + 1)/2$ ensures the convergence of the series, while the coefficients $\langle P_l \rangle$ are the orientation factors determined experimentally. The first even-order Legendre polynomials are given by:

$$\langle P_0 \rangle = 1 \tag{11a}$$

$$\langle P_2 \rangle = \frac{(3\langle \cos^2\theta \rangle - 1)}{2} \tag{11b}$$

$$\langle P_4 \rangle = \frac{(35\langle \cos^4\theta \rangle - 30\langle \cos^2\theta \rangle + 3)}{8} \tag{11c}$$

The infrared spectroscopy allows the calculation of the $\langle P_2 \rangle$ coefficient. This coefficient, called order parameter, is related to the dichroic ratios $R_{(\alpha=0)}^{T}$ and $R_{(\alpha=0)}^{ATR}$ by the relation:

$$\langle P_2 \rangle = \frac{R_{(\alpha=0)}^{T,ATR} - 1}{R_{(\alpha=0)}^{T,ATR} + 2} \tag{12}$$

The order parameter $\langle P_2 \rangle$ ranges from 1.0 for $\theta = 0°$ (all the long molecular axes of the mesogens are aligned parallel to the rubbing direction) to −0.5 (all the long molecular axes of the mesogens are aligned perpendicular to the rubbing direction). For the special case of $\langle P_2 \rangle = 0$, the orientation can be interpreted as an isotropic distribution of the long molecular axes or as a delta distribution centered at $\theta = 54.7°$.

Polarized Raman measurements provide both $\langle P_2 \rangle$ and $\langle P_4 \rangle$ parameters in the distribution function $f(\theta)$. Since the theoretical background has been discussed thoroughly in ref 11, we simply review the results. If we consider vibrations along the long molecular axis, such as C═C stretching vibrations of the phenyl rings, the Raman scattering tensor can be written in a diagonal form as

$$\vec{\alpha}_{mol} = \alpha_{zz} \begin{pmatrix} a & 0 & 0 \\ 0 & a & 0 \\ 0 & 0 & 1 \end{pmatrix} \tag{13}$$

Notice that the z axis is parallel to the long molecular axis and that $a = \alpha_{xx}/\alpha_{zz}$. The depolarization ratio observed in the isotropic phase allows us to determine the value of a:

$$R_{iso} = \frac{I_{VH}}{I_{VV}} = \frac{(1-a)^2}{3 + 4a + 8a^2} \cong \frac{1}{3}\left(1 - \frac{10}{3}a\right) \tag{14}$$

Since it is not straightforward to achieve an isotropic polymerization of liquid crystal polymers, we measured R_{iso} on an isotropic sample of monomers.

Chart 1. Microphotography of the Lattice of Defect Lines[a]

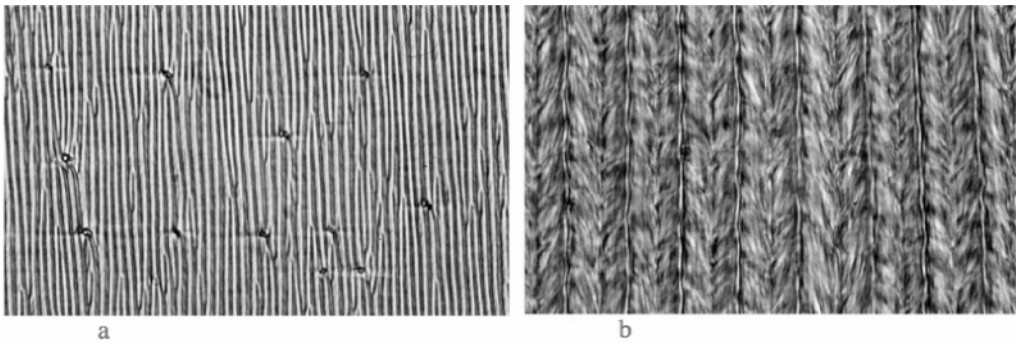

[a] Key: (a) Observed on a thin film (7 μm). (b) Observed on a thick film (63 μm).

Then, the depolarization ratios in the nematic phase are given by

$$R_1 = \frac{I_{ZY}}{I_{ZZ}} = \frac{D^2 C_N}{8} \frac{\langle \cos^2\theta \rangle - \langle \cos^4\theta \rangle}{\frac{1}{9} - \frac{D}{9} + \frac{D^2}{36} + \left(\frac{D}{3} - \frac{D^2}{6}\right)\langle \cos^2\theta \rangle + \frac{D^2}{4}\langle \cos^4\theta \rangle} \quad (15)$$

$$R_2 = \frac{I_{YZ}}{I_{YY}} = \frac{D^2}{8C_N} \frac{\langle \cos^2\theta \rangle - \langle \cos^4\theta \rangle}{\frac{1}{9} + \frac{D}{18} + \frac{11D^2}{288} - \left(\frac{D}{6} + \frac{5D^2}{48}\right)\langle \cos^2\theta \rangle + \frac{3D^2}{32}\langle \cos^4\theta \rangle} \quad (16)$$

where

$$D = \frac{2 - 2a}{1 + 2a} = \frac{7 + 9R_{iso}}{8 - 9R_{iso}}$$

C_N is a correction factor for transmission loss and is given by

$$C_N = \left(\frac{n_s + n_e}{n_s + n_o}\right)^2 \quad (17)$$

where n_s is the refractive index of the substrate and n_o and n_e are the ordinary and extraordinary refractive indexes of the sample, respectively.

The $\langle P_2 \rangle$ and $\langle P_4 \rangle$ order parameters can be easily calculated from eqs 15−17. However, since the spectroscopic techniques cannot provide all the $\langle P_l \rangle$ parameters, the series expansion of eq 10 is not always converging. Nevertheless, following Berne et al.,[21] it is possible to estimate the most probable orientational distribution function by using the information entropy theory. Introducing the Lagrange' multipliers λ_2 and λ_4, the following expression of the most probable and normalized distribution function $f_{mp}(\theta)$ is given by:

$$f_{mp}(\theta) = \frac{\exp[\lambda_2 P_2 \cos\theta + \lambda_4 P_4 \cos\theta]}{\int_0^\pi \exp[\lambda_2 P_2 \cos\theta + \lambda_4 P_4 \cos\theta] \sin\theta \, d\theta} \quad (18)$$

For uniaxial orientation centered parallel to a reference direction, i.e., behaving a positive $\langle P_2 \rangle$ value within the (0, 1) range, Pottel et al.[22] have demonstrated that three distinct domains can be distinguished in the ($\langle P_2 \rangle$,$\langle P_4 \rangle$) half-plane and they lead to different typical shapes of the orientational distribution functions. More precisely, for any $\langle P_2 \rangle$ value and increasing $\langle P_4 \rangle$ ones, one encounters a first domain of unimodal asymmetric functions (cone model), a second domain of Gaussian distribution (centered at 0°) and a third domain of bimodal shape functions (centered at 0° and 90°).

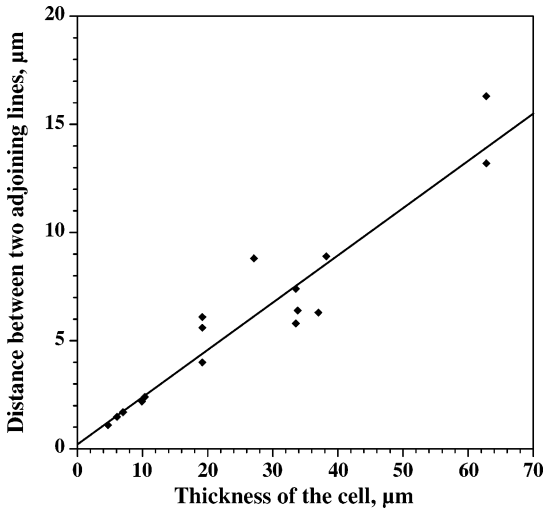

Figure 2. Distance between two adjoigning lines measured from microscopic observations on polymerized film vs the film thickness.

Results

Microscopy. Textures and polarization states have been determined by microscopy. Textures are the elements forming the "landscape" and polarization state is the result of the interaction between the polarized light and the film. Some cells have been observed before polymerization. The nematic liquid crystal monomer is very well oriented. This is stated by a perfect extinction, between crossed polarizers, when the rubbing direction D is parallel to the polarizer P or the analyzer A and also by the fact that no texture can be observed.

The texture of a polymerized film displays a periodic lattice of lines perpendicular to D. Chart 1a shows the lattice of a thin film (≈7 μm) and Chart 1b that of a thick film (≈63 μm). The periodicity of the lattices (i.e., the distance between two adjoining lines) has been measured for samples of various thicknesses. The periodicity is a linear function of the film thickness, as shown in Figure 2. In thick cells (beyond about 10 μm) a "chevron" texture is inserted between the lines (Chart 1b). At strong magnifications these lines are visible even with-

Chart 2. Effect of the Temperature on the Lattice of Lines[a]

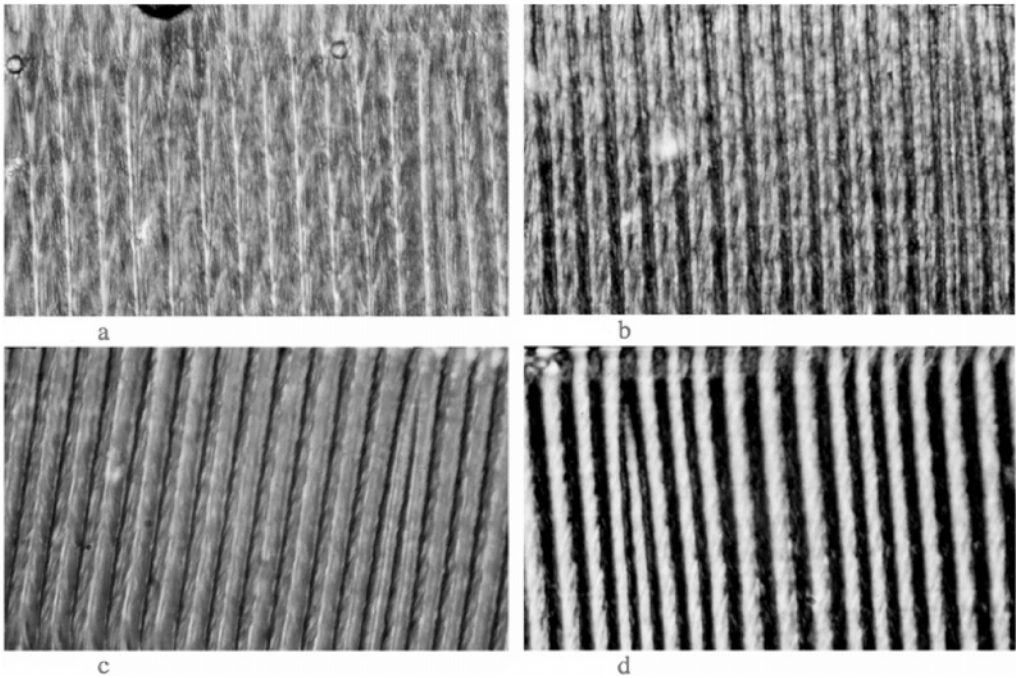

[a] At 22 °C (a), at 85 °C (b), at 118 °C (c), 2 °C before the nematic−isotropic transition, and at 130 °C (d), in the isotropic state.

out polarizers, they have a submicron diameter and are located at specific levels. A very regular periodical lattice of such lines is located close to the surfaces of the film. However, the larger the thickness and the more numerous the lines located in the bulk, besides the periodical lattice. These lines in the bulk are less easily focused.

The polarization state is also quite different for thin and thick films. There is a quasi-extinction of the light between crossed polarizers, with D parallel to P or A, when the film thickness is smaller than 5 μm. With D at 45° of P and A, the polarization color is a white or a first-order gray in the Newton scale. By contrast, no extinction is possible when the thickness is larger than 5 μm: whatever the relative positions of P and A are, the field is colored. The rotation of the film between crossed polarizers or the rotation of the analyzer with respect to the polarizer change the color but do not permit one to reach the extinction. Colors are brighter than in the previous case.

To probe the effect of the temperature on the texture and on the polarization state, we used films still included between the substrates. The nematic−isotropic transition of the polymer occurs at 120 °C. Starting from 22 °C (Chart 2a) and increasing the temperature up to 20 deg above the transition, we do not observe any change of the periodicity. However, the lines located in the bulk seem to disappear progressively. In a first step, the lines located near the surface become softer and then a network of light and dark fringes replaces the lines. Chart 2b shows the texture at 85 °C, Chart 2c at 118 °C (i.e. 2° before the transition) and Chart 2d at 130 °C. The texture does not change at higher temperatures. Decreasing the temperature down to 22 °C restores the texture previously observed.

All these observations show that the lines are topological defects called disclination lines. These lines are the places where the discontinuity concentrates when the director **n** changes its direction. At the time of polymerization a volume shrinkage occurs, inducing a contraction. Because of the contraction, the mesogenic parts of the polymer probably tip up. We will see below that this interpretation is well supported by the vibrational spectroscopy results.

Table 1. Assignment, Frequency, and Dichroic Ratio of the Major Bands in the Infrared Spectra of the Oriented Polymer in the Nematic State[a]

assignment	freq (cm^{-1})	R^T	R^{ATR}
ν(C=O)	1732	1.045[b]	1.168
ν(C=C)$_{Ar}$ (ν_{8a})	1606	1.438	4.066
ν(C=C)$_{Ar}$ (ν_{8b})	1580	1.690	4.000
ν(C=C)$_{Ar}$ (ν_{19a})	1511	1.494	3.894
ν(C=C)$_{Ar}$ (ν_{19b})	1422	1.579	3.359
ν_a(C−O−C) in Ar−CO−O−Ar′	1255	1.160[b]	2.935
ν_a(C−O−C) in Ar−CO−O−R	1165	1.167[b]	3.024
ν_s(C−O−C) in Ar−CO−O−Ar′	1066	1.347[b]	2.518
δ_{op}(=C−H) in 1,4-disubstituted benzenes	847	0.634	0.532
δ_{op}(=C−H) in 1,2,4-trisubstituted benzenes	762	0.663	0.517
δ_{op}(=C−H) in 1,4-disubstituted benzenes	692	0.653	0.476

[a] Key: ν = stretching vibration, δ_{op} = out-of-plane bending vibration, a = asymmetric, s = symmetric, and Ar = aromatic. [b] Estimated values of the dichroic ratio since the polarized absorbances are higher than 1.5.

FTIR Spectroscopy. The polarized transmittance spectra in the 1800−600 cm^{-1} region of free-standing thin film (6 μm thick) of oriented polymer (nematic state) are presented in Figure 3a for a radiation polarized parallel and perpendicular to the rubbing direction. The assignment of the main absorption bands in these spectra is summarized in Table 1. The infrared spectra of the hydrogenated polymer exhibit some bands characteristic of the mesogen groups. For example, the bands due to the ν(C=C) stretching vibrations of the phenyl rings occur at 1606, 1580, 1511, and 1422 cm^{-1}, whereas the bands due to the C−O−C asymmetric stretching vibration, ν_a(C−O−C), of the Ar−CO−O−Ar′ and Ar−CO−O−R groups occur at 1255 and 1165 cm^{-1}.[23] The bands associated with the stretching vibrations of the phenyl rings have been used to determine the orientation of the mesogens since their transition moments are expected to have the same direction than the long molecular axis of the mesogens ($\alpha \approx 0°$). The bands located at 847, 762, and 692 cm^{-1} are characteristic of the out-

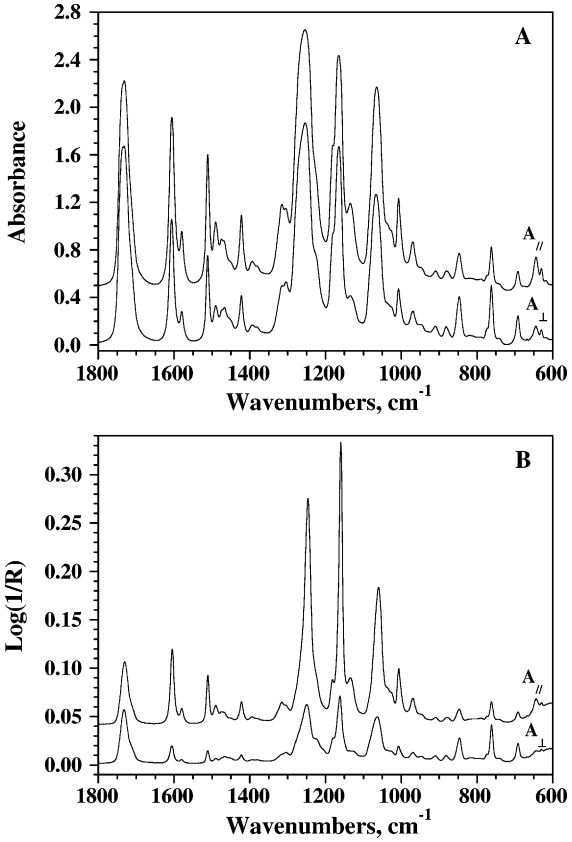

Figure 3. Typical polarized absorbance (A) and ATR (B) spectra of a polymerized film of thickness 6 μm, recorded with the electric field of the radiation polarized parallel and perpendicular to the rubbing direction.

of-plane =C−H deformation of the disubstituted (847 and 692 cm^{-1}) and trisubstituted (762 cm^{-1}) phenyl rings.[23] The investigation of these bands is very interesting since their transition moments are perpendicular to the ring plane ($\alpha = 90°$), allowing a better understanding of the molecular orientation of the mesogen groups. Finally, the intense band at 1732 cm^{-1} is assigned to the ν(C=O) stretching vibrations of both the mesogen and spacer groups. It is important to notice that, in the deuterated polymer, the bands due to the asymmetric ($\nu_a(CD_2)$) and symmetric ($\nu_s(CD_2)$) stretching vibrations are observed at 2219 and 2113 cm^{-1}, respectively. Their investigation allows the determination of the backbone orientation in the liquid-crystal elastomer.

The dichroic ratios are easily calculated for the different bands using eq 3, and the corresponding values are gathered in Table 1. For the four modes corresponding to the ν(C=C) stretching vibrations of the phenyl rings, the values are found larger than 1, over a restricted range [1.44−1.69]. The three modes corresponding to the out-of-plane deformation of the phenyl rings have also similar values but the dichroic ratio is significantly lower than 1. The similar values calculated for the 762 cm^{-1} band characteristic of the 1,2,4-trisubstituted phenyl rings and for the two other bands (at 847 and 692 cm^{-1}) associated with the 1,4-para-substituted phenyl rings indicate that the three phenyl rings are almost in the same plane. In the following, the average of the dichroic ratio of the 1606, 1580, 1511, and 1422 cm^{-1} bands have been considered to calculate the tilt angle θ between the long molecular axis of the mesogens and the rubbing direction. Similarly, the average of the dichroic ratio of the 847, 762, and 692 cm^{-1} bands have been calculated to determine the orientation of the phenyl ring plane with respect to the film plane (Y, Z plane in Scheme 2).

The polarized ATR spectra of the same thin polymer film are presented in Figure 3b in the 1800−600 cm^{-1} region for a radiation polarized perpendicular to the plane of incidence and for the sample positioned with the rubbing direction parallel and perpendicular to the polarization direction, respectively. The band intensities are one order smaller than those observed on the transmittance spectra since the evanescent wave occurring in ATR experiments does not penetrate the sample deeply. As mentioned in the theoretical section, the probed thickness can be estimated from the depth of penetration d_p. This parameter can be easily calculated by eq 9, considering the refractive indexes of the various media ($n_1 = 4.0$ for the germanium crystal and $n_2 = 1.6$ for the film) and the angle of incidence ($\Phi = 45°$). Values of 0.455 and 0.910 μm are found for bands located at 1500 and 750 cm^{-1}, respectively. Consequently, polarized ATR experiments provide information about the molecular orientation of the mesogen groups near the surface of the polymer film. The values of the dichroic ratio calculated for the ν(C=C) stretching vibrations of the phenyl rings are very high (close to 4), indicating a much better orientation (near the polymer film surface) of the mesogen groups with respect to the rubbing direction.

The order parameter $\langle P_2 \rangle$, calculated from the dichroic ratios $R^{T}_{(\alpha=0)}$ and $R^{ATR}_{(\alpha=0)}$ using eq 12, are reported in Table 2 for hydrogenated and deuterated polymer films of various thicknesses. The results obtained from transmittance experiments show that the average mesogen orientation is only slightly modified by the thickness of the film when this thickness is lower than 15 μm (thin films). Likewise, no significant variations are observed in ATR results, indicating that the molecular orientation near the surface is not affected by the thickness of the samples. The average values of the order parameters are reported in Table 3a for the transmittance and ATR experiments. The results obtained for the ν(C=C) stretching vibrations of the phenyl rings indicate that the long molecular axis of the mesogen groups is preferentially oriented parallel to the rubbing direction (order parameter positive) and that this orientation is better near the surface of the polymer film. This last point is not surprising since the surface of the film was in contact with the rubbing layer. The anchoring effect produced by the rubbing layer associated with the volume shrinkage during the polymerization induces a non homogeneous orientation of the mesogen groups near the surface of the film which is certainly correlated with the topological defects observed by microscopic observations. In the other hand, the order parameter values calculated for the out-of-plane =C−H deformation of the phenyl rings are similar for transmittance and ATR experiments. The negative values of the order parameter were expected since the transition moments of these bands are perpendicular to the long molecular axis of the mesogens, but its magnitude indicates clearly a non-cylindrical symmetry of the phenyl rings with respect to the long molecular axis. Indeed, for a perfect cylindrical symmetry, the following relation should be achieved:

$$\langle P_2(\cos\theta)\rangle_{\delta_{op}(=C-H)} = -\frac{\langle P_2(\cos\theta)\rangle_{\nu(C=C)}}{2} \qquad (19)$$

Table 2. Dichroic Ratios and Order Parameters $\langle P_2 \rangle$ of Different Functional Groups for Hydrogenated and Deuterated Polymer Films of Various Thicknesses

	Transmittance Experiments					
	6 μm, H[a]		7 μm, H[a]		13.2 μm, D[a]	
	R^T	P_2	R^T	P_2	R^T	P_2
ν(C=C)$_{Ar}$	1.551 ± 0.038	0.155 ± 0.008	1.729 ± 0.035	0.195 ± 0.008	1.751 ± 0.077	0.200 ± 0.016
δ_{op}(=C−H)	0.650 ± 0.012	−0.132 ± 0.005	0.556 ± 0.017	−0.174 ± 0.007	0.334 ± 0.033	−0.286 ± 0.019
ν(C−D)					0.537	−0.183
ν(C=O)	1.045	0.015	1.009	0.003	0.925	−0.026

	ATR Experiments							
	6 μm, H[a]		19.2 μm, D[a]		26.3 μm, D[a]		33.5 μm, D[a]	
	R^{ATR}	P_2	R^{ATR}	P_2	R^{ATR}	P_2	R^{ATR}	P_2
ν(C=C)$_{Ar}$	3.987 ± 0.070	0.499 ± 0.006	4.744 ± 0.159	0.555 ± 0.010	5.115 ± 0.096	0.578 ± 0.005	4.379 ± 0.070	0.530 ± 0.005
δ_{op}(=C−H)	0.508 ± 0.024	−0.196 ± 0.011	0.416 ± 0.028	−0.242 ± 0.014	0.461 ± 0.029	−0.219 ± 0.014	0.484 ± 0.028	−0.208 ± 0.014
ν(C−D)			0.818	−0.065	0.936	−0.022	0.898	−0.035
ν(C=O)	1.168	0.053	1.167	0.053	1.272	0.083	1.201	0.063

[a] H: hydrogenated polymer. D: deuterated polymer.

Table 3. Parameters Calculated from Transmittance and ATR Experiments

	transmittance	ATR
(a) Average Values of the Order Parameters $\langle P_2 \rangle$		
ν(C=C)$_{Ar}$	0.183 ± 0.020	0.541 ± 0.029
δ_{op}(=C−H)	−0.197 ± 0.065	−0.216 ± 0.017
ν(C−D)	−0.183	−0.041 ± 0.018
ν(C=O)	−0.003 ± 0.017	0.063 ± 0.012
(b) Tilt Angle θ and Twist Angle ψ of the Mesogen Groups[a]		
θ (deg)	47.5	33.5
ψ (deg)	52.2	38.0

[a] With respect to the rubbing direction.

Nevertheless, if we consider an uniaxial orientation of the long molecular axis of the mesogen groups and a non cylindrical symmetry of the phenyl rings with respect to the rubbing direction, the orientation of the phenyl ring plane with respect to the film plane (twist angle ψ) can be calculated from eq 6, assuming an infinitely narrow distribution of orientation. Values of this angle are reported in Table 3b for transmittance and ATR experiments. The phenyl ring plane is preferentially parallel to the film plane near the surface ($\psi < 45°$ for ATR) whereas it is preferentially perpendicular to the film plane inside the film ($\psi > 45°$ for transmittance). By contrast with the ν(C=C) results, the order parameters obtained for ν(C−D) bands are negative and close to zero for the ATR experiments. Since the transition moments of $\nu_a(CD_2)$ and $\nu_s(CD_2)$ vibrations are perpendicular to the main chain direction of the polymer, the backbone orientation is preferentially parallel to the rubbing direction. Moreover, the main chains present a poorer orientation when the mesogen groups are better oriented. This suggests that the backbone orientation adapts to the mesogen orientation. A good orientation of the mesogen groups prevents a good orientation of the main chains. Finally, the order parameter value of the carbonyl band is close to 0, indicating a random orientation of its transition moment. This feature is certainly due to the fact that the carbonyl group is present both in the mesogen and in the spacer.

Polarized transmittance spectra on films placed between BaF_2 plates with rubbed PVA surface have been recorded at various temperatures to probe the molecular orientation of the mesogen groups at the nematic−isotropic transition. Order parameter values for the 1422 and 847 cm^{-1} bands are reported in Figure 4 between 25 and 140 °C. The values obtained at 30 °C for a confined sample in the nematic phase are similar than those reported in Table 2 for free-standing films. In the nematic state (between 30 and 115 °C), the order parameters increase slightly (in absolute value) with the temperature up to 90 °C and more rapidly above 90 °C. This result can be explained by a larger mobility of the mesogen groups. The order parameters decreases sharply near the nematic−isotropic transition temperature (T_{NI}) which has been estimated at 119 °C from differential scanning calorimetry.[6] However, the value of $\langle P_2 \rangle$ in the isotropic phase does not go to zero but retains a finite value (0.034) due to the network. It is important to notice that relation 19 seems to be valid for temperature higher than T_{NI}, indicating a cylindrical symmetry of the phenyl rings in the isotropic phase. Finally, when the sample is cooled back to room temperature, initial values of the order parameters are found again (see open symbols in Figure 4), demonstrating the thermal reversibility of the mesogen orientation (network memory).

Raman Spectroscopy. A set of typical polarized Raman spectra for a thick film (71.6 μm) of oriented polymer is presented in Figure 5 between 1500 and 1800 cm^{-1}. The spectra are dominated by two main peaks located at about 1600 and 1728 cm^{-1}, assigned to the

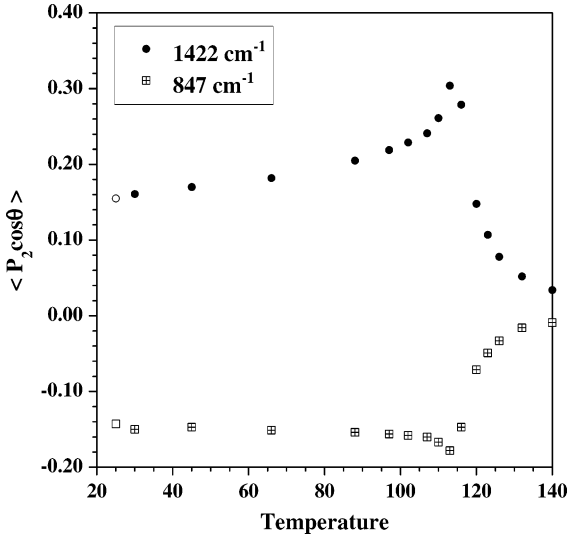

Figure 4. Plot of the parameter order $\langle P_2 \rangle$ of a polymerized film for the 1422 and 847 cm^{-1} bands as a function of temperature through the isotropic to nematic phase transition.

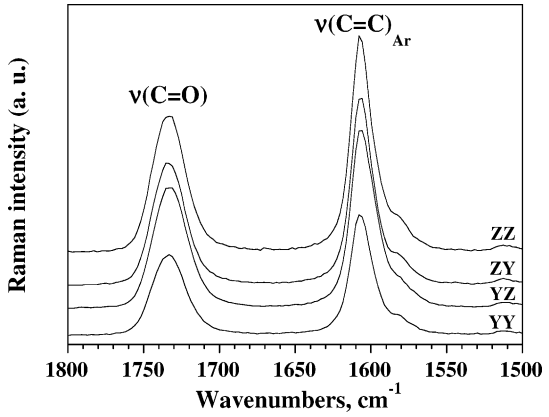

Figure 5. Typical polarized Raman spectra of a polymerized film of thickness 71.6 μm, in the frequency range of the C=C stretching modes of the phenyl rings. The spectra were arbitrarily shifted along the *Y*-axis for clarity. From top to bottom, *ZZ*, *ZY*, *YZ*, and *YY* configurations.

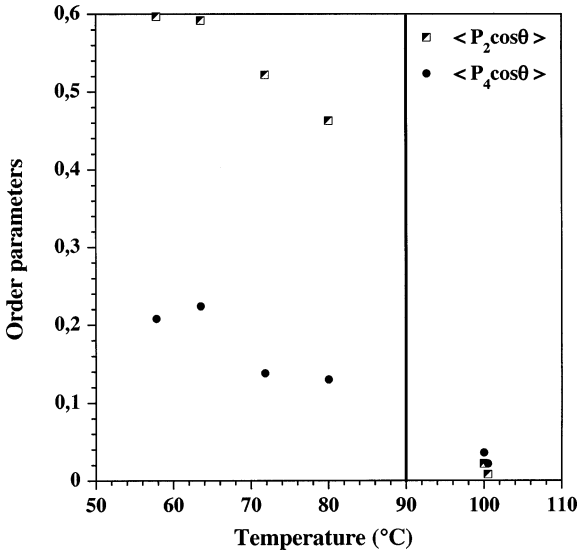

Figure 6. Temperature dependence of the $\langle P_2 \rangle$ and $\langle P_4 \rangle$ order parameters of the mesogens for the monomer. The vertical line indicates the nematic−isotropic transition.

ν(C=C) stretching mode of the phenyl rings and the ν-(C=O) stretching mode, respectively. In the following, we focus on the analysis of the ν(C=C) stretching mode. It is generally accepted that the average stretching direction of the phenyl rings is parallel to the long molecular axis of the mesogens and that the Raman tensor has a diagonal form with only two different nonzero values $\alpha_{xx} = \alpha_{yy} \neq \alpha_{zz}$.[11] As mentioned in the theoretical section, one can get a description of the orientational order of the long molecular axis of the mesogens ($\langle P_2 \rangle$ and $\langle P_4 \rangle$ order parameters in the following) through the analysis of the polarization dependence of the Raman intensities of the ν(C=C) stretching mode. Note that, as expected for a diagonal Raman tensor, the intensities in *ZY* and *YZ* configurations are equal.

In a first step, the consistency of our data treatment has been checked by studying the samples before polymerization, i.e., in the monomer form, as a function of temperature from nematic to isotropic phase. The values of the order parameters calculated from the two depolarization ratios $R_1 = I_{ZY}/I_{ZZ}$ and $R_2 = I_{YZ}/I_{YY}$ are presented in Figure 6. As mentioned above, these order parameters are characteristic of the orientation of the long molecular axis of the mesogens. $\langle P_2 \rangle$ and $\langle P_4 \rangle$ are found to decrease monotically when the temperature increases and to go down to zero in the isotropic phase, as expected. The values of the order parameters and the Lagrange' multipliers λ_2 and λ_4 are given in Table 4 for three temperatures and the corresponding most probable distribution functions $f_{mp}(\theta)$ are displayed in Figure 7a. They correspond well to what is expected for a nematic distribution, i.e., a distribution which goes through a maximum in the rubbing direction (0°) and which decreases continuously for angles perpendicular to the alignment direction (Gaussian distribution). When the temperature increases, the distribution function becomes flat and is nearly constant above the nematic−isotropic transition temperature. Note that for a perfect random orientation ($\langle P_2 \rangle = \langle P_4 \rangle = 0$), the most probable distribution function should be equal to 0.5 over all the angles.

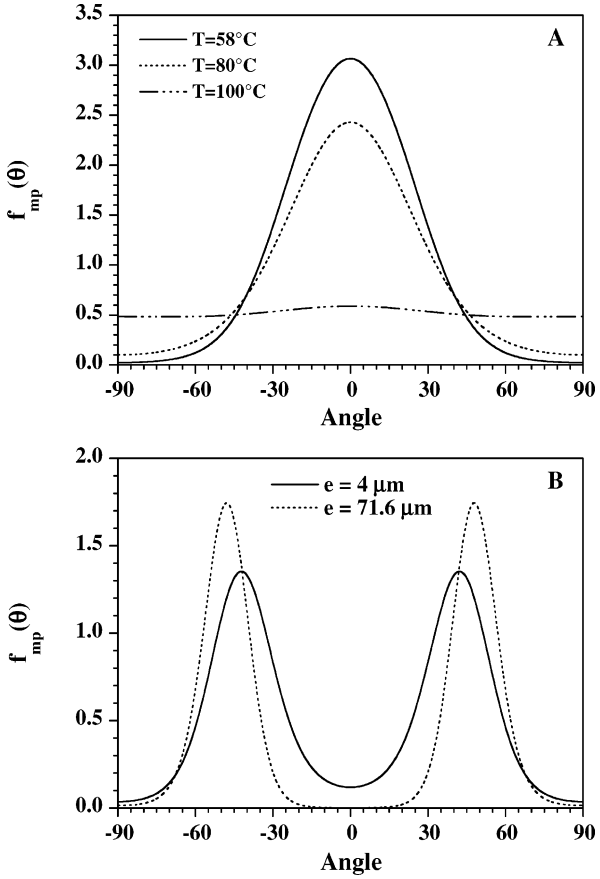

Figure 7. Most probable distribution functions $f_{mp}(\theta)$ of the mesogens for the monomer at different temperatures (A) and polymer cells of different thicknesses (B).

Table 4. Order Parameters P_2 and P_4 and Lagrange Multipliers λ_2 and λ_4 for Samples before Polymerization (in the monomer form) at Different Temperatures and after Polymerization for Different Film Thicknesses

		P_2	P_4	λ_2	λ_4
monomer	$T = 58°$ C	0.60	0.20	3.459	−0.516
	$T = 80$ °C	0.46	0.13	2.151	−0.705
	$T = 100$°C	0.022	0.007	0.106	0.058
polymer	$e = 4$ μm	0.24	−0.22	1.925	−2.736
	$e = 71.6$ μm	0.13	−0.33	0.672	−5.417

We achieved measurements for about 20 different cells of different thicknesses, and the results are presented in Figure 8. For all polymer samples, the $\langle P_2 \rangle$ and $\langle P_4 \rangle$ order parameters strongly differ than those of the monomer in the nematic phase, signifying an

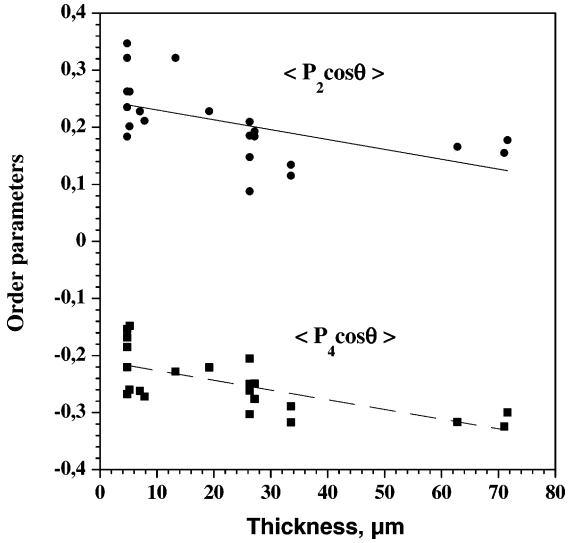

Figure 8. Order parameters for a series of polymer cells, as a function of the thickness cell.

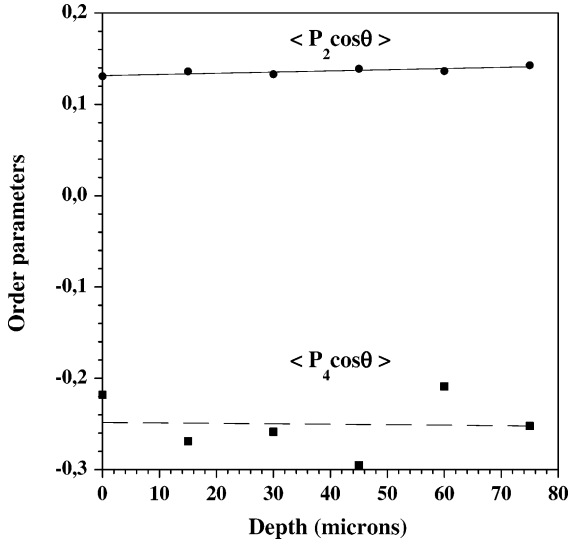

Figure 9. Depth dependence of the order parameters for a thick cell, as measured from Raman confocal experiments.

important change in the distribution of the orientation function of the mesogen groups. Moreover, the negative values of $\langle P_4 \rangle$ indicate that the distribution goes through a maximum for a nonzero angle (cone model). The values obtained for $\langle P_2 \rangle$ order parameter range between 0.14 and 0.24, in agreement with the values obtained from transmittance experiments. Moreover, a slight but significant decrease of the order parameters is observed when the cell thickness increases. Typical distribution functions $f_{mp}(\theta)$ are plotted in Figure 7b for thin ($e = 4$ μm) and thick ($e = 71.6$ μm) polymer films. The shape of the function is relevant and significantly different from that of the monomer; the distribution function goes through a maximum at about 45°. Furthermore, the smaller the order parameters and the sharper the maximum of the distribution function. For thick films, the values of $\langle P_4 \rangle$ are close to the values of $\langle P_4 \rangle_{min} = 1/18(35\langle P_2 \rangle^2 - 10\langle P_2 \rangle - 7)$,[22] revealing a narrow distribution of orientation. For large order parameters, which correspond to the thinner film ($e = 4$ μm), the distribution of orientation spreads over a large angular range, which is in agreement with modifications of the mesogen orientation from the surface to the bulk, as suggested by FTIR experiments. For thick samples, even if similar changes are expected, the distribution function is dominated by the contribution of the bulk. This indicates that a good orientation along the rubbing direction is only achieved for a thin layer close to the surface. This result is supported by Raman confocal measurements at different depths in thick cells as shown in Figure 9. Since the axial resolution in these experiments was about 8 μm,[16] no depth dependence has been observed.

Discussion

In microscopic observations, the quasi-extinction of the thin films for the director *D* parallel to P or A shows that the director **n** is in the XOZ plane, but not in the *YOZ* plane. To interpret the disclination lines, correlated to the extinction, we propose the sketch of Figure 10. Figure 10a is a section of the structure parallel to *XOZ*. The small segments in Figure 10a show the director in the plane of the figure, the small circles describe the lines perpendicular to the plane, where the discontinuity of the director is located. Figure 10b is a section parallel to *YOZ*. The most distant lines are the disclination lines, the other ones show the field of the director projection in the plane. Near the surfaces, we assume that the director remains in the *YOZ* plane. We cannot explain the periodicity and its relation with the thickness. Other parameters probably play a role, like elastic constants and viscosity.

In thick samples, because of the regular lattice of lines correlated to the "chevron" texture and to the loss of extinction, we assume that during the contraction the director not only leaves the *YOZ* plane but also the *XOZ* plane. The distribution of the director is described by the sketch of Figure 10, parts c and d. In Figure 10c the nails represent the directors cutting the plane of the figure, the tip is the projection of the director on the plane and the head indicates the place where the director cuts the plane. In Figure 10d, the curves show the field of the projection of the director, explaining the "chevron" texture.

The dark and light fringes observed at higher temperatures can be explained by the fact that the polymer chains, although aligned in average along *D*, follow the contraction. In the isotropic state the mesogenic parts are in disorder but the polymer remains nearly aligned, keeping some memory of the periodical lattice.

This very simple interpretation is limited to the region close to the surfaces. It does not intend to describe the distribution of the director in the whole film. However, this interpretation seems to be supported by the vibrational spectroscopy results. Indeed, ATR experiments have shown clearly a higher orientation of the mesogen groups near the film surface because of the anchoring effect of the rubbing layer. Inside the polymer, we have shown from transmittance experiments (using the out-of-plane =C−H deformation of the phenyl rings) that the mesogens move away from the rubbing direction with a non perfect cylindrical symmetry. A more precise estimation of the orientation distribution functions has been obtained using polarized Raman scattering since this technique allows the determination of both $\langle P_2 \rangle$ and $\langle P_4 \rangle$ order parameters. From these order parameters, we have calculated a narrow distribution function for the mesogen groups, with a maximum centered at 48° from the rubbing direction. This value is characteristic of the internal part of the samples because of the low axial resolution of the Raman technique.

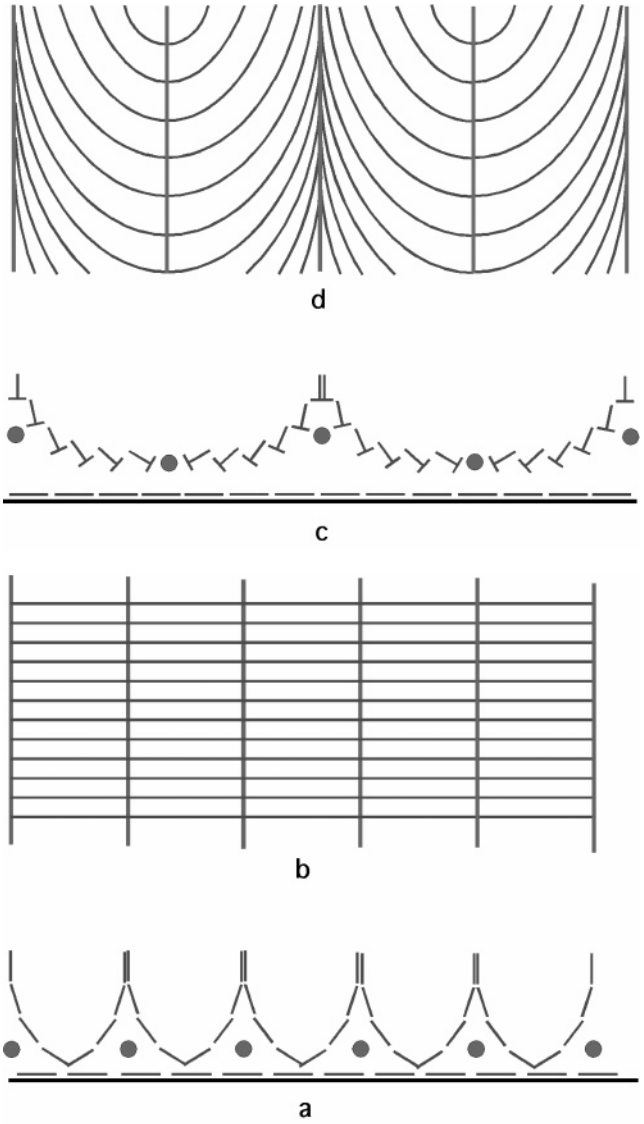

Figure 10. Model of the director orientation drawn from microscopic observations on polymerized thin films in the *XOZ* (a, side view) and *YOZ* (b, top view) planes and on thick films in the *XOZ* (c, side view) and *YOZ* (d, top view) planes.

FTIR spectroscopy has been used also to determine both the mesogen and backbone orientations, using the dichroic comportment of the ν(C=C) component and the ν(C−D) stretching vibrations of deuterated main chains, respectively. Surprisingly, the study of the partially deuterated polymer films has shown that the backbone orientation was rather good inside the polymer whereas it was poor near the surface where the mesogens are well oriented. This suggests that the backbone orientation adapts to the mesogen orientation. Therefore, near the surface, the mesogen orientation is driven mainly by the rubbing surface interaction, involving a disorganized backbone orientation. In contrast, inside the sample, the steric and dipole−dipole repulsive effects of the mesogens become predominant inducing an extension and a better orientation of the backbone. All these results suggest that the non homogeneous mesogen orientation between the surface and the internal part of the film is certainly correlated with the disclination lines observed by microscopic observations. Indeed, these topological defects can be explained by discontinuities where the director changes its direction. Finally, FTIR experiments performed at different temperatures have evidenced the cylindrical symmetry of the mesogens above the nematic−isotropic transition temperature, the residual mesogen orientation in the isotropic phase, the mesogen orientation memory in the nematic phase but also a pretransition reorientation induced by the relaxation of the polymer constraint at higher temperature.

Conclusion

In this study, we have investigated the molecular orientation in liquid crystal elastomers. Microscopic observations revealed complex texture and polarization states. FTIR spectroscopy was used to determine both the mesogen and backbone orientations, using the dichroic comportment of the ν(C=C) stretching vibrations of the phenyl rings and the ν(C−D) stretching vibrations of deuterated main chains, respectively. Transmittance experiments have been performed to probe molecular orientation on the whole film whereas pertinent information near the film surface has been obtained from attenuated total reflectance experiments. A more precise estimation of the orientation distribution functions has been obtained using polarized Raman scattering since this technique allows the determination of both $\langle P_2 \rangle$ and $\langle P_4 \rangle$ order parameters. An orientation model has been proposed to explain the spectroscopic results as well as the microscopic observations. This model shows clearly that the long molecular axis of the mesogen groups is not homogeneously oriented in the polymer films. Except near the surface, in the major part of the polymer this orientation is not along the rubbing direction as expected with the film preparation. This orientation model also explain why the macroscopic contraction measured on this liquid crystal elastomer at the nematic−isotropic transition is weaker than that expected from theoretical predictions. Indeed, due to the tilt orientation of the mesogen groups in the nematic phase, the polymer film cannot reach its highest extension and therefore the change at the transition proceeds only between a partial extended polymer and an isotropic organization.

Acknowledgment. The authors are indebted to the Ministry of Research (ACI 2000 "Physico-chimie de la matière complexe"), to the CNRS (Chemistry Department) and to Région Aquitaine for financial support. They are thankful to C. Sourisseau for several fruitful discussions and to F. Lagugné-Labarthet for distribution function calculations.

References and Notes

(1) de Gennes, P.-G. *Phys. Lett.* **1969**, *A 28*, 725.
(2) Brand, H. R.; Finkelmann, H. In *Physical Properties of Liquid Crystalline Elastomers*; Demus, D., Ed.; Wiley VCH: New York, 1998; pp 227−302.
(3) Warner, M.; Terentjev, E. M. In *Liquid Crystal Elastomers*; Oxford University Press: Oxford, England, 2003.
(4) de Gennes, P.-G. *C. R. Acad. Sci. Paris Ser. II* **1997**, *324*, 343.
(5) Wermter, H.; Finkelmann, H. *e-polym*. **2001**, 013 (www.e-Polym..org).
(6) Thomsen, D. L.; Keller, P.; Naciri, J.; Pink, R.; Jeon, H.; Shenoy, D.; Ratna, B. R. *Macromolecules* **2001**, *34*, 5868.
(7) Clarke, S. M.; Hotta, A.; Tajbakhsh, A. R.; Terentjev, E. M. *Phys. Rev. E* **2001**, *64*, 61702.
(8) (a) Leroux, N.; Keller, P.; Achard, M. F.; Noirez, L.; Hardouin, F. *J. Phys. II* **1993**, *3*, 1289. (b) Leroux, N.; Achard, M. F.; Keller, P.; Hardouin, F. *Liq. Cryst.* **1994**, *16*, 1073.

(9) (a) Braeuchler, M.; Boeffel, C.; Spiess, H. W. *Makromolekulare Chemie* **1991**, *192*, 1153. (b) Wiesner, U.; Reynolds, N.; Boeffel, C.; Spiess, H. W. *Liq. Cryst.* **1992**, *11*, 251.
(10) Mirabella, F. M. In *Internal Reflection Spectroscopy*; Mirabella, F. M., Ed.; Marcel Dekker: New York, 1993; pp 17−52.
(11) Jen, S.; Clark, N. A.; Pershan, P. S.; Priestley, E. B. *J. Chem. Phys.* **1977**, *66*, 4635.
(12) Miyano, K. *J. Chem. Phys.* **1978**, *69*, 4807.
(13) Kim, K. H.; Miyachi, K.; Ishikawa, K.; Takezoe, H.; Fukuda, A. *Jpn. J. Appl. Phys.* **1994**, *33*, 5850.
(14) Gautier, P.; Brunet, M.; Grupp, J.; Sauvajol, J. L.; Anglaret, E. *Phys. Rev. E* **2000**, *62*, 7528.
(15) Keller, P.; Thomsen, D. L.; Li, M. H. *Macromolecules* **2002**, *35*, 581.
(16) Bruneel, J. L.; Lassègues, J. C.; Sourisseau, C. *J. Raman Spectrosc.* **2002**, *33*, 815.
(17) Zbinden, R. In *Infrared Spectroscopy of High Polymers*; Academic Press: New York, 1964, Chapter 5.
(18) Harrick, N. J.; du Pré, F. K. *Appl. Opt.* **1966**, *5*, 1739.
(19) Stein, R. S. *J. Polym. Sci.* **1958**, *31*, 327.
(20) Samuels, R. J. In *Structured Polymer Properties*; Interscience: New York, 1974.
(21) Berne, B. J.; Pechukas, P.; Harp, G. D. *J. Chem. Phys.* **1968**, *49*, 3125.
(22) Pottel, H.; Herreman, W.; Van deer Meer, B. W.; Ameloot, M. *Chem. Phys.* **1986**, *102*, 37.
(23) Socrates, G. *In Infrared Characteristic Group Frequencies*; Wiley-Interscience Publication: New York, 1980.

MA050136N